JACS
JOURNAL OF THE AMERICAN CHEMICAL SOCIETY
pubs.acs.org/JACS
Communication

Spectroelectrochemistry of Water Oxidation Kinetics in Molecular versus Heterogeneous Oxide Iridium Electrocatalysts

Carlota Bozal-Ginesta, Reshma R. Rao, Camilo A. Mesa, Yuanxing Wang, Yanyan Zhao, Gongfang Hu, Daniel Antón-García, Ifan E. L. Stephens, Erwin Reisner, Gary W. Brudvig, Dunwei Wang, and James R. Durrant*

Cite This: J. Am. Chem. Soc. 2022, 144, 8454–8459

ABSTRACT: Water oxidation is the step limiting the efficiency of electrocatalytic hydrogen production from water. Spectroelectrochemical analyses are employed to make a direct comparison of water oxidation reaction kinetics between a molecular catalyst, the dimeric iridium catalyst $[Ir_2(pyalc)_2(H_2O)_4\text{-}(\mu\text{-}O)]^{2+}$ ($\mathbf{Ir_{Molecular}}$, pyalc = 2-(2′pyridinyl)-2-propanolate) immobilized on a mesoporous indium tin oxide (ITO) substrate, with that of an heterogeneous electrocatalyst, an amorphous hydrous iridium ($\mathbf{IrO_x}$) film. For both systems, four analogous redox states were detected, with the formation of Ir(4+)−Ir(5+) being the potential-determining step in both cases. However, the two systems exhibit distinct water oxidation reaction kinetics, with potential-independent first-order kinetics for $\mathbf{Ir_{Molecular}}$ contrasting with potential-dependent kinetics for $\mathbf{IrO_x}$. This is attributed to water oxidation on the heterogeneous catalyst requiring co-operative effects between neighboring oxidized Ir centers. The ability of $\mathbf{Ir_{Molecular}}$ to drive water oxidation without such co-operative effects is explained by the specific coordination environment around its Ir centers. These distinctions between molecular and heterogeneous reaction kinetics are shown to explain the differences observed in their water oxidation electrocatalytic performance under different potential conditions.

Water oxidation catalysis is a key challenge for hydrogen synthesis from water via electrolysis, with extensive interest in both heterogeneous oxides and molecular catalysts.[1−3] While heterogeneous oxides are already employed in commercial electrolyzers, there have been striking recent advances in the performance and stability of molecular water oxidation catalysts based on iridium.[4−7] Molecular catalysts are particularly attractive as model systems for this reaction, with their well-defined and tunable atomic structures aiding mechanistic insight.[7−10] A key potential mechanistic difference is that molecular catalysts typically consist of isolated metal centers, while heterogeneous oxide films are often reported to promote water oxidation by co-operative effects between adjacent sites.[11−13] Recent work has controversially suggested that long-range interactions, which depend on the coverage of oxidized *O species, can be attributed to solvation effects on IrO_x surfaces.[11] However, direct comparisons between the water oxidation kinetics of molecular and heterogeneous catalysts operating under similar reaction conditions have been very limited to date.[14,15] Herein we use *operando* transient spectroelectrochemistry to compare two highly active water-oxidation electrocatalysts based on iridium: a dimeric molecular catalyst $[Ir_2(pyalc)_2(H_2O)_4\text{-}(\mu\text{-}O)]^{2+}$ ($\mathbf{Ir_{Molecular}}$, Figure 1A) (pyalc = 2-(2′pyridinyl)-2-propanolate) and the amorphous hydrous iridium oxide ($\mathbf{IrO_x}$, Figure 1B).[2,3,7,16−20]

It has previously been reported that molecular iridium catalysts can be immobilized on oxide surfaces without the need for additional anchoring groups. When immobilized on high-surface area mesoporous indium tin oxide (mesoITO), $\mathbf{Ir_{Molecular}}$ can reach turnover frequencies around 7.9 s^{-1} at an overpotential of 520 mV, and its ligands remain intact for at least 11 h at pH 2.6 under 1.55 V_{RHE}.[16] $\mathbf{Ir_{Molecular}}$ cocatalysts have also been reported to enhance the performance of hematite photoanodes, shifting the oxygen evolution reaction (OER) onset potential by ∼250 mV.[14,15,21] In our previous work on $\mathbf{IrO_x}$ electrodes, spectroelectrochemical techniques were applied to identify three redox transitions, attributed following the literature to the oxidation of Ir^{3+} to $Ir^{3.x+}$, $Ir^{3.x+}$ to Ir^{4+}, and Ir^{4+} to $Ir^{4.y+}$, where $Ir^{3.x+}$ and $Ir^{4.y+}$ represent mixed valence states including Ir^{3+} and Ir^{4+}, and oxidized Ir^{4+} respectively.[22−39] The final redox transition results in the formation of oxygenated species, *O, whose OER kinetics can also be probed using time-resolved spectroelectrochemistry.[22] Herein, we extend this spectroelectrochemical analysis to the dimeric complex $\mathbf{Ir_{Molecular}}$ immobilized on mesoITO. By comparing the molecular redox states and their kinetics to those of electrodeposited $\mathbf{IrO_x}$ films,[22] we aim to understand the impact on OER activity of the specific coordination environment of iridium centers in $\mathbf{Ir_{Molecular}}$ as well as the potential impact of co-operative effects between Ir centers present in the heterogeneous $\mathbf{IrO_x}$ film.

The molecular iridium catalyst $\mathbf{Ir_{Molecular}}$ was immobilized on mesoporous ITO (mesoITO) following a previously reported

Received: February 22, 2022
Published: May 5, 2022

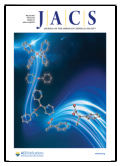

https://doi.org/10.1021/jacs.2c02006
J. Am. Chem. Soc. 2022, 144, 8454−8459

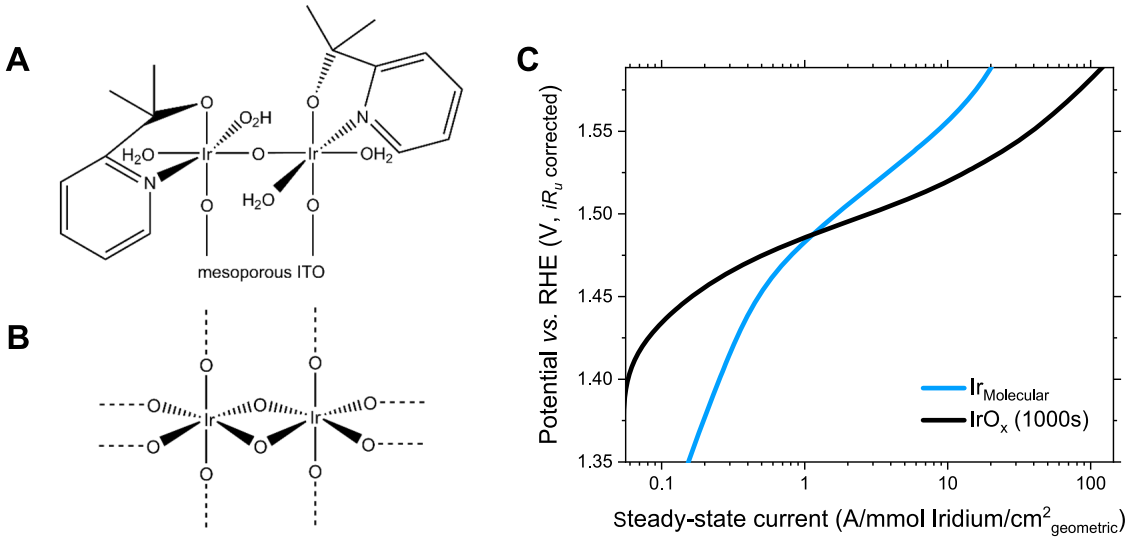

Figure 1. (A) Proposed molecular structure of $\mathbf{Ir}_{\mathbf{Molecular}}$ and (B) schematic of a cluster in electrodeposited $\mathbf{IrO}_x$, proposed by Pavlovic et al.[13,20,21] (C) Tafel plot from the steady-state current per mol of electrochemically active iridium every 50 mV of $\mathbf{Ir}_{\mathbf{Molecular}}$ and $\mathbf{IrO}_x$ (electrodeposited for 1000s) in aqueous $HClO_4$ 0.1 M at pH 1.2. The calculation of electrochemically active iridium is described in the Supporting Information.

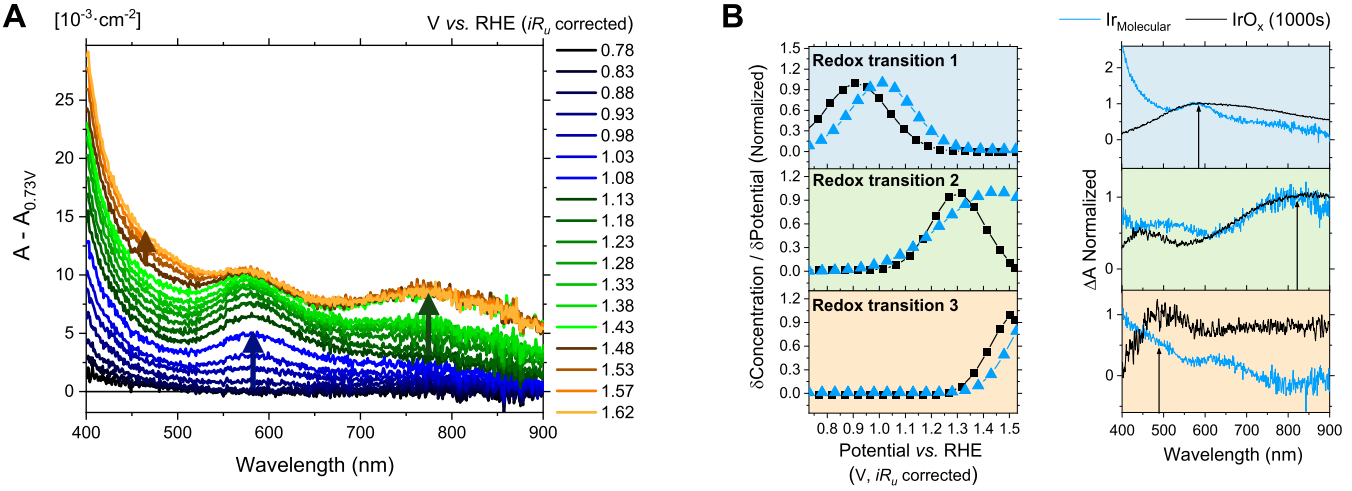

Figure 2. (A) Absorption changes at different potentials of $\mathbf{Ir}_{\mathbf{Molecular}}$ on mesoporous ITO. (B) Normalized deconvolution results of the spectroelectrochemical data of $\mathbf{Ir}_{\mathbf{Molecular}}$ and $\mathbf{IrO}_x$: (*left*) change in the concentration of the redox states formed at increasing potentials and (*right*) differential absorption coefficients of the corresponding redox transitions (relative to 0.73 V vs RHE). Measurements done in aqueous $HClO_4$ 0.1 M at pH 1.2 under constant applied potentials every 0.05 V.

procedure, forming a packed monolayer of ~0.04 $\mu mol_{Ir}/cm^2_{geometric}$, while $\mathbf{IrO}_x$ films were electrodeposited in water from an iridium salt.[14−16] Iridium centers in mesoITO-$\mathbf{Ir}_{\mathbf{Molecular}}$ are expected to be at least 3 times further away from the iridium centers in adjacent molecules than between iridium centers in one $\mathbf{Ir}_{\mathbf{Molecular}}$ catalyst and in $\mathbf{IrO}_x$ because of the bulkiness of the ligands.[14,16] The Tafel plot of the resulting $\mathbf{Ir}_{\mathbf{Molecular}}$ films (Figure 1C) shows an exponential increase in the[26,27] current at a potential of ~1.32 V_{RHE}, ~80 mV lower than in $\mathbf{IrO}_x$. Comparing the catalytic waves for water oxidation in Figure 1C, the $\mathbf{Ir}_{\mathbf{Molecular}}$ films exhibit higher performance below ~1.45 V_{RHE} with a Tafel slope of 174 mV/dec. Above 1.45 V_{RHE}, $\mathbf{IrO}_x$ films exhibit a sharper onset and thus higher performance than $\mathbf{Ir}_{\mathbf{Molecular}}$, with Tafel slopes of 59 and 69 mV/dec, respectively, in accordance with previous studies.[11,16]

The redox chemistry of $\mathbf{Ir}_{\mathbf{Molecular}}$ on mesoITO was analyzed further spectroelectrochemically, following procedures we have previously reported for $\mathbf{IrO}_x$ (Figures S2−S3).[22] Its UV−vis absorption spectrum was measured as a function of applied potential with 5 mV increments in aqueous 0.1 M $HClO_4$ electrolyte at pH 1.2 (Figure 2A). For the potential range 0.78−1.08 V_{RHE}, an absorption band at 590 nm dominated the spectrum. A new feature appeared at 800 nm between 1.13 and 1.43 V_{RHE}, and above 1.43 V_{RHE}, absorption changes were primarily detected below 500 nm. These features were deconvolved (Figures 2B and S3−S7) by fitting a model which assumes three additive contributions to the absorption, each linearly proportional to the concentration of redox states, and where the concentration of redox states formed at each potential follows a Gaussian distribution (SI, Equations S2−7), as reported in our previous work.[22] The deconvoluted spectroelectrochemistry results are shown in Figure 2B, where the normalized concentration distributions and differential absorption corresponding to the three redox transitions detected in $\mathbf{Ir}_{\mathbf{Molecular}}$ are compared to those in $\mathbf{IrO}_x$. The

https://doi.org/10.1021/jacs.2c02006
J. Am. Chem. Soc. 2022, 144, 8454−8459

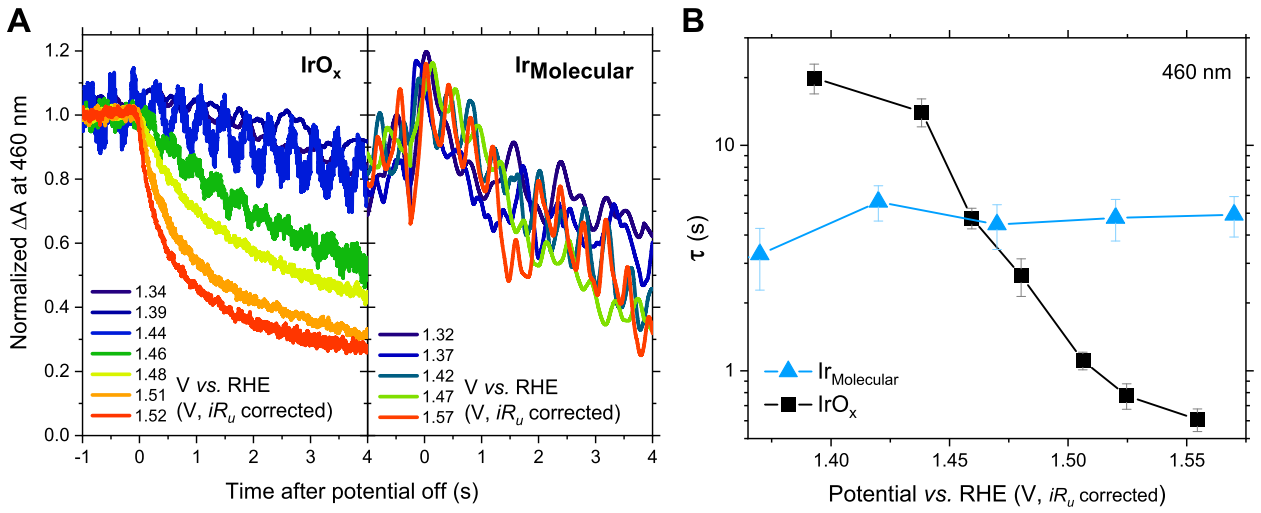

Figure 3. (A) Absorption decay after turning the potential off, and (B) optical signal lifetimes derived from fitting an initial linear regression in Figure 3A in $\mathbf{Ir_{Molecular}}$ and $\mathbf{IrO_x}$ in 0.1 M $HClO_4$ water at pH 1.2.

optical signals related to the three redox transitions in the two catalysts have broadly similar features (Figure 2B left). However, the absorption bands are slightly blue-shifted in $\mathbf{Ir_{Molecular}}$ (shown in more detail in Figure S8). The concentration distributions in $\mathbf{Ir_{Molecular}}$ are shifted anodically by ∼100 mV with respect to $\mathbf{IrO_x}$ for all the three redox transitions (Figure 2B right).

Considering the assignments of the redox transitions in Figure 2 for $\mathbf{IrO_x}$, the transitions in the 0.8−1.4 V_{RHE} range have been assigned to intervalence charge transfer within the iridium d orbitals derived from the oxidation of Ir(3+) to Ir(4+) and deprotonation of hydroxyl groups coordinated to the Ir center.[23,24,32,35,40−42] Positive of 1.4 V_{RHE}, redox states of iridium higher than 4+ are expected to be formed.[29,33,34,43−45] Crabtree et al. have reported similar redox transitions in an iridium dimer structurally analogous to $\mathbf{Ir_{Molecular}}$: Ir(3+)−Ir(3+) absorbing below 450 nm, Ir(4+)−Ir(4+) absorbing at 600−750 nm, and Ir(4+)−Ir(5+) absorbing at 500 nm.[46,47] By taking this iridium dimer as a reference, the three redox transitions we observe in $\mathbf{Ir_{Molecular}}$ can be assigned to the sequential oxidation of Ir(3+)−Ir(3+) to Ir(3+)−Ir(4+), Ir(4+)−Ir(4+), and Ir(4+)−Ir(5+), respectively, in good agreement with assignments on $\mathbf{IrO_x}$. The absolute absorption and the calculated concentrations are smaller for mesoITO-$\mathbf{Ir_{Molecular}}$ compared to electrodeposited $\mathbf{IrO_x}$ (Figures 2A and S7 for $\mathbf{Ir_{Molecular}}$ and S1B and S2 for $\mathbf{IrO_x}$), indicative of larger geometric densities of electrochemically active Ir centers in $\mathbf{IrO_x}$, and attributed to its permeability to the electrolyte and electrode morphology. By comparing the electrochemical and the deconvoluted spectroelectrochemical data in Figures 1C and 2B, respectively, it is apparent for both $\mathbf{Ir_{Molecular}}$ and $\mathbf{IrO_x}$ that the electrocatalytic current overlaps with the third redox transition detected spectroelectrochemically (discussed further below). This indicates that this transition, assigned to Ir(4+)−Ir(5+) formation in $\mathbf{Ir_{Molecular}}$, enables O_2 evolution, similar to our findings on $\mathbf{IrO_x}$. It is also apparent that this transition is shifted anodically for the $\mathbf{Ir_{Molecular}}$ relative to $\mathbf{IrO_x}$, indicative of the role of ligands in tuning the redox activity of the Ir centers.

To analyze the kinetics of the redox states in $\mathbf{Ir_{Molecular}}$, the optical signal decay was measured after turning an applied potential off, following the same procedure reported for $\mathbf{IrO_x}$ in our previous study (Scheme S1 and Supporting Information).[22] This methodology was used to deduce the OER reaction kinetics of the active redox state as a function of its concentration. Absorption changes upon applying an electric potential from the open circuit potential (OCP) were detected only at applied potentials above ∼1.32 V_{RHE} (iR_u corrected) (Figure 3A), which corresponds to the potential at which the active redox state Ir(4+)−Ir(5+) is formed. Notably, the decay kinetics of the active state optical signal in $\mathbf{Ir_{Molecular}}$ are almost invariant throughout the 1.3−1.6 V_{RHE} range, implying a potential-independent first-order mechanism, where the rate of the reaction (J) is proportional to a potential-independent rate constant (k) and the concentration of oxidized species (θ); i.e., $J = k\theta$. This contrasts with the behavior of $\mathbf{IrO_x}$, where the decay of the optical signal becomes substantially faster with increasing potentials in this range. The corresponding decay time constants are plotted in Figure 3B, where the optical signal lifetimes at different potentials were extracted from fitting the signal decays with an initial linear regression (Equations S10−S11). It is apparent that, at potentials below 1.45 V_{RHE}, the lifetimes of the active state in $\mathbf{IrO_x}$ are longer than in $\mathbf{Ir_{Molecular}}$, indicative of lower reactivity, while above 1.45 V_{RHE} the lifetimes become shorter, indicative of higher reactivity.

Apart from the shift in oxidation potential discussed above, $\mathbf{IrO_x}$ and $\mathbf{Ir_{Molecular}}$ show similar potential dependencies for the third redox transition assigned to the formation of the oxidized species driving OER (Figure 2B). As such, the smaller Tafel slope observed for $\mathbf{IrO_x}$ (Figure 2A) can be assigned to a sharper acceleration of OER reaction kinetics for this film with potential. The absence of any potential dependence of reaction kinetics for $\mathbf{Ir_{Molecular}}$ suggests that this acceleration for $\mathbf{IrO_x}$ is unlikely to be due to a mechanism change or potential-dependent change in reaction activation energy.

For $\mathbf{Ir_{Molecular}}$ the third redox transition (Figure 2B) coincides with the potential required to reach 0.1 A/mmol/$cm^2_{geometric}$ (Figure 1C), consistent with its first-order OER kinetics. In contrast, for $\mathbf{IrO_x}$ the potential to reach 0.1 A/mmol/$cm^2_{geometric}$ is shifted anodically by ∼100 mV relative to its third redox transition, providing further confirmation that this heterogeneous catalyst needs to reach a critical concentration of redox active state to trigger the OER reaction.

https://doi.org/10.1021/jacs.2c02006
J. Am. Chem. Soc. 2022, 144, 8454−8459

Therefore, it appears likely that this acceleration results from co-operative effects between different oxidized Ir centers on $\mathbf{IrO}_x$,[48] consistent with a recent report by Nong et al.[11] of co-operative interactions between multiple sites on IrO_x during OER. Such co-operative effects cannot be realized in the isolated Ir centers of mesoITO-$\mathbf{Ir}_{\mathbf{Molecular}}$ due to steric hindrance by the ligands.

At low overpotentials, in the absence of co-operative effects that can enhance OER activity on $\mathbf{IrO}_x$, the reactivity for both catalysts would be governed by the chemical environment of isolated oxidized Ir centers, including the ligands and the electrode substrate, as illustrated in Scheme 1. In the molecular

Scheme 1. Proposed Chemical Effects of the Atoms Coordinated to the Iridium Active Sites on the Redox Potential (E) and Maximum Absorption Wavelength of d−d Transitions ($\lambda_{max.}$(d−d)), and lifetimes (τ) in water 0.1 M $HClO_4$ at pH 1.2

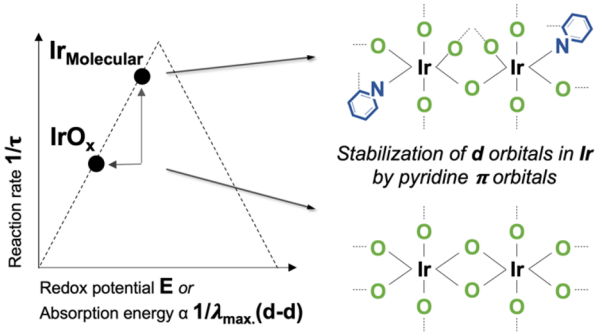

catalyst, the absorption maxima above 500 nm are slightly blue-shifted (Figure 2B right), and the potential for each redox transition in $\mathbf{Ir}_{\mathbf{Molecular}}$ is shifted by ∼100 mV compared to $\mathbf{IrO}_x$ (Figure 2B left). Considering that the Ir centers have an octahedral configuration in both $\mathbf{Ir}_{\mathbf{Molecular}}$ and $\mathbf{IrO}_x$, a plausible cause for these shifts is different solvation environment in $\mathbf{Ir}_{\mathbf{Molecular}}$ and $\mathbf{IrO}_x$ and the stabilization of the t_{2g} d-based iridium molecular orbitals in $\mathbf{Ir}_{\mathbf{Molecular}}$ by pyridine π orbitals (Scheme 1).[49,50] On the one hand, this would lead to a larger energy gap between the t_{2g} and e_g molecular orbitals, which corresponds to the transition observed in the visible range.[49,50] On the other hand, this stabilization of the t_{2g} molecular orbitals, where the valence electrons are located, would make the iridium centers in $\mathbf{Ir}_{\mathbf{Molecular}}$ harder to oxidize than in $\mathbf{IrO}_x$. This is in agreement with the seminal work of Rossmeisl and Nørskov et al.[51] which suggested that IrO_2(110) binds oxygen too strongly relative to the optimal catalyst, resulting in the O−O bond formation step to form *OOH being rate-determining. Consequently, the faster reaction kinetics, and higher OER activity of $\mathbf{Ir}_{\mathbf{Molecular}}$ at low overpotentials (<1.45 V_{RHE}), can thus be explained by the stabilization effect of the pyridine ligand on the valence iridium d orbitals, which increases the oxidizing potential of Ir and decreases the oxygen binding strength.

In conclusion, by employing *operando* spectroelectrochemistry, we have analyzed the redox transitions and OER reaction kinetics for $\mathbf{IrO}_x$ and for $\mathbf{Ir}_{\mathbf{Molecular}}$ immobilized on meso-ITO between 1 and 1.6 V_{RHE}. The third redox transition, assigned in both systems to Ir(4+) oxidation, was observed to correlate with the increase in the OER current. $\mathbf{Ir}_{\mathbf{Molecular}}$ is observed to exhibit potential independent OER reaction kinetics, indicative of water oxidation by independent molecular catalysts. This contrasts with $\mathbf{IrO}_x$ films, where the reaction kinetics are observed to accelerate strongly with applied potential, attributed to the OER on this catalyst requiring co-operative interactions between neighboring oxidized Ir centers. The ability of $\mathbf{Ir}_{\mathbf{Molecular}}$ to drive OER without requiring such co-operative effects is attributed to the anodic shift of its redox transitions relative to $\mathbf{IrO}_x$, resulting from the specific chemical environment of its iridium centers. These differences in redox state energetics and OER kinetics explain the differences observed in OER activity and Tafel slopes between these molecular and heterogeneous catalysts. The absence of co-operative effects, as observed herein for our molecular system, could limit the performance of single atom catalysts[52−55] for OER, particularly on Ir-based centers. Our study has therefore allowed a direct comparison of molecular catalysts and heterogeneous oxide film OER kinetics, thus providing insights into how both the local environment of the catalytic site and co-operative effects between oxidized sites can result in significantly different water oxidation kinetics.

■ ASSOCIATED CONTENT

Supporting Information

The Supporting Information is available free of charge at https://pubs.acs.org/doi/10.1021/jacs.2c02006.

Preparation and measurement procedures, Scheme S1, Equations S1−S9, Figures S1−S14, and Table S1. All the raw data are available on Zenodo (10.5281/zenodo.6407221). (PDF)

■ AUTHOR INFORMATION

Corresponding Author

James R. Durrant − *Department of Chemistry, Centre for Processable Electronics, Imperial College London, London W12 0BZ, U.K.;* orcid.org/0000-0001-8353-7345; Email: j.durrant@imperial.ac.uk

Authors

Carlota Bozal-Ginesta − *Department of Chemistry, Centre for Processable Electronics, Imperial College London, London W12 0BZ, U.K.;* Present Address: C.B.G.: Departments of Chemistry and Computer Science, University of Toronto, Lash Miller Chemical Laboratories, 80 St. George Street, M5S3H6 Toronto, Canada; orcid.org/0000-0001-7299-5869

Reshma R. Rao − *Department of Chemistry, Centre for Processable Electronics, Imperial College London, London W12 0BZ, U.K.;* orcid.org/0000-0002-6655-3105

Camilo A. Mesa − *Department of Chemistry, Centre for Processable Electronics, Imperial College London, London W12 0BZ, U.K.;* Present Address: C.A.M.: Institute of Advanced Materials (INAM), Universitat Jaume I, Avenida de Vicent Sos Baynat, s/n, 12006 Castelló de la Plana, Spain; orcid.org/0000-0002-8450-2563

Yuanxing Wang − *Department of Chemistry, Boston College, Chestnut Hill, Massachusetts 02467, United States;* orcid.org/0000-0003-3742-7238

Yanyan Zhao − *Department of Chemistry, Boston College, Chestnut Hill, Massachusetts 02467, United States;* orcid.org/0000-0002-1428-5022

Gongfang Hu − *Yale Energy Sciences Institute and Department of Chemistry, Yale University, New Haven,*

https://doi.org/10.1021/jacs.2c02006
J. Am. Chem. Soc. 2022, 144, 8454−8459

Connecticut 06520, United States; orcid.org/0000-0002-0387-9079

Daniel Antón-García − *Yusuf Hamied Department of Chemistry, University of Cambridge, Cambridge CB2 1EW, U.K.*

Ifan E. L. Stephens − *Department of Materials, Imperial College London, London W12 0BZ, U.K.;* orcid.org/0000-0003-2157-492X

Erwin Reisner − *Yusuf Hamied Department of Chemistry, University of Cambridge, Cambridge CB2 1EW, U.K.;* orcid.org/0000-0002-7781-1616

Gary W. Brudvig − *Yale Energy Sciences Institute and Department of Chemistry, Yale University, New Haven, Connecticut 06520, United States;* orcid.org/0000-0002-7040-1892

Dunwei Wang − *Department of Chemistry, Boston College, Chestnut Hill, Massachusetts 02467, United States;* orcid.org/0000-0001-5581-8799

Complete contact information is available at: https://pubs.acs.org/10.1021/jacs.2c02006

Notes

The authors declare no competing financial interest.

■ ACKNOWLEDGMENTS

J.R.D., I.E.L.S., and R.R.R. acknowledge funding from bp-ICAM. C.B-G. was supported by an EPSRC DTP studentship. Work at Yale University and Boston College was supported by the U.S. Department of Energy, Chemical Sciences, Geosciences, and Biosciences Division, Office of Basic Energy Sciences, Office of Science (Grant DEFG02-07ER15909 and Grant DE-SC0020261, respectively). D.A.G. acknowledges funding from an EPSRC PhD DTA studentship (EP/M508007/1).

■ REFERENCES

(1) Bernt, M.; Siebel, A.; Gasteiger, H. A. Analysis of Voltage Losses in PEM Water Electrolyzers with Low Platinum Group Metal Loadings. *J. Electrochem. Soc.* **2018**, *165* (5), F305−F314.

(2) Seh, Z. W.; Kibsgaard, J.; Dickens, C. F.; Chorkendorff, I.; Nørskov, J. K.; Jaramillo, T. F. Combining Theory and Experiment in Electrocatalysis: Insights into Materials Design. *Science* **2017**, *355* (6321). DOI: 10.1126/science.aad4998.

(3) Haussener, S.; Xiang, C.; Spurgeon, J. M.; Ardo, S.; Lewis, N. S.; Weber, A. Z. Modeling, Simulation, and Design Criteria for Photoelectrochemical Water-Splitting Systems. *Energy Environ. Sci.* **2012**, *5* (12), 9922.

(4) Taibi, E.; Blanco, H.; Miranda, R.; Carmo, M.; Gielen, D.; Roesch, R. Green Hydrogen Cost Reduction: Scaling up Electrolysers to Meet the 1.5°C Climate Goal. *International Renewable Energy Agency* 2020, ISBN: 978-92-9260-295-6.

(5) Zhang, B.; Sun, L. Artificial Photosynthesis: Opportunities and Challenges of Molecular Catalysts. *Chem. Soc. Rev.* **2019**, *48* (7), 2216−2264.

(6) Matheu, R.; Garrido-Barros, P.; Gil-Sepulcre, M.; Ertem, M. Z.; Sala, X.; Gimbert-Suriñach, C.; Llobet, A. The Development of Molecular Water Oxidation Catalysts. *Nat. Rev. Chem.* **2019**, *3* (5), 331−341.

(7) Thomsen, J. M.; Huang, D. L.; Crabtree, R. H.; Brudvig, G. W. Iridium-Based Complexes for Water Oxidation. *Dalton Trans* **2015**, *44* (28), 12452−12472.

(8) McDaniel, N. D.; Coughlin, F. J.; Tinker, L. L.; Bernhard, S. Cyclometalated Iridium(III) Aquo Complexes: Efficient and Tunable Catalysts for the Homogeneous Oxidation of Water. *J. Am. Chem. Soc.* **2008**, *130* (1), 210−217.

(9) Savini, A.; Bellachioma, G.; Ciancaleoni, G.; Zuccaccia, C.; Zuccaccia, D.; Macchioni, A. Iridium(III) Molecular Catalysts for Water Oxidation: The Simpler the Faster. *Chem. Commun.* **2010**, *46* (48), 9218−9219.

(10) van Dijk, B.; Rodriguez, G. M.; Wu, L.; Hofmann, J. P.; Macchioni, A.; Hetterscheid, D. G. H. The Influence of the Ligand in the Iridium Mediated Electrocatalyic Water Oxidation. *ACS Catal.* **2020**, *10* (7), 4398−4410.

(11) Nong, H. N.; Falling, L. J.; Bergmann, A.; Klingenhof, M.; Tran, H. P.; Spori, C.; Mom, R.; Timoshenko, J.; Zichittella, G.; Knop-Gericke, A.; Piccinin, S.; Perez-Ramirez, J.; Cuenya, B. R.; Schlögl, R.; Strasser, P.; Teschner, D.; Jones, T. E. Key Role of Chemistry versus Bias in Electrocatalytic Oxygen Evolution. *Nature* **2020**, *587* (7834), 408−413.

(12) Francàs, L.; Corby, S.; Selim, S.; Lee, D.; Mesa, C. A.; Godin, R.; Pastor, E.; Stephens, I. E. L.; Choi, K. S.; Durrant, J. R. Spectroelectrochemical Study of Water Oxidation on Nickel and Iron Oxyhydroxide Electrocatalysts. *Nat. Commun.* **2019**, *10* (1), 5208.

(13) Mesa, C. A.; Francàs, L.; Yang, K. R.; Garrido-Barros, P.; Pastor, E.; Ma, Y.; Kafizas, A.; Rosser, T. E.; Mayer, M. T.; Reisner, E.; Grätzel, M.; Batista, V. S.; Durrant, J. R. Multihole Water Oxidation Catalysis on Haematite Photoanodes Revealed by Operando Spectroelectrochemistry and DFT. *Nat. Chem.* **2020**, *12*, 82−89.

(14) Li, W.; He, D.; Sheehan, S. W.; He, Y.; Thorne, J. E.; Yao, X.; Brudvig, G. W.; Wang, D. Comparison of Heterogenized Molecular and Heterogeneous Oxide Catalysts for Photoelectrochemical Water Oxidation. *Energy Environ. Sci.* **2016**, *9* (5), 1794−1802.

(15) Li, W.; Sheehan, S. W.; He, D.; He, Y.; Yao, X.; Grimm, R. L.; Brudvig, G. W.; Wang, D. Hematite-Based Solar Water Splitting in Acidic Solutions: Functionalization by Mono- and Multilayers of Iridium Oxygen-Evolution Catalysts. *Angew. Chem., Int. Ed. Engl.* **2015**, *54* (39), 11428−11432.

(16) Sheehan, S. W.; Thomsen, J. M.; Hintermair, U.; Crabtree, R. H.; Brudvig, G. W.; Schmuttenmaer, C. A. A Molecular Catalyst for Water Oxidation That Binds to Metal Oxide Surfaces. *Nat. Commun.* **2015**, *6*, 6469.

(17) Frydendal, R.; Paoli, E. A.; Knudsen, B. P.; Wickman, B.; Malacrida, P.; Stephens, I. E. L.; Chorkendorff, I. Benchmarking the Stability of Oxygen Evolution Reaction Catalysts: The Importance of Monitoring Mass Losses. *ChemElectroChem.* **2014**, *1* (12), 2075−2081.

(18) Wei, C.; Rao, R. R.; Peng, J.; Huang, B.; Stephens, I. E. L.; Risch, M.; Xu, Z. J.; Shao-Horn, Y. Recommended Practices and Benchmark Activity for Hydrogen and Oxygen Electrocatalysis in Water Splitting and Fuel Cells. *Adv. Mater.* **2019**, *31* (31), No. 1806296.

(19) Marshall, A.; Børresen, B.; Hagen, G.; Tsypkin, M.; Tunold, R. Hydrogen Production by Advanced Proton Exchange Membrane (PEM) Water Electrolysers—Reduced Energy Consumption by Improved Electrocatalysis. *Energy* **2007**, *32* (4), 431−436.

(20) Carmo, M.; Fritz, D. L.; Mergel, J.; Stolten, D. A Comprehensive Review on PEM Water Electrolysis. *Int. J. Hydrog. Energy* **2013**, *38* (12), 4901−4934.

(21) Badia-Bou, L.; Mas-Marza, E.; Rodenas, P.; Barea, E. M.; Fabregat-Santiago, F.; Gimenez, S.; Peris, E.; Bisquert, J. Water Oxidation at Hematite Photoelectrodes with an Iridium-Based Catalyst. *J. Phys. Chem. C* **2013**, *117* (8), 3826−3833.

(22) Bozal-Ginesta, C.; Rao, R. R.; Mesa, C. A.; Liu, X.; Hillman, S. A. J.; Stephens, I. E. L.; Durrant, J. R. Redox-State Kinetics in Water-Oxidation IrOx Electrocatalysts Measured by Operando Spectroelectrochemistry. *ACS Catal.* **2021**, *11* (24), 15013−15025.

(23) Ooka, H.; Wang, Y.; Yamaguchi, A.; Hatakeyama, M.; Nakamura, S.; Hashimoto, K.; Nakamura, R. Legitimate Intermediates of Oxygen Evolution on Iridium Oxide Revealed by in Situ Electrochemical Evanescent Wave Spectroscopy. *Phys. Chem. Chem. Phys.* **2016**, *18* (22), 15199−15204.

(24) Ooka, H.; Takashima, T.; Yamaguchi, A.; Hayashi, T.; Nakamura, R. Element Strategy of Oxygen Evolution Electrocatalysis

Based on in Situ Spectroelectrochemistry. *Chem. Commun. Camb* **2017**, *53* (53), 7149−7161.
(25) Nahor, G. S.; Hapiot, P.; Neta, P.; Harriman, A. Changes in the Redox State of Iridium Oxide Clusters and Their Relation to Catalytic Water Oxidation: Radiolytic and Electrochemical Studies. *J. Phys. Chem.* **1991**, *95* (2), 616−621.
(26) Pavlovic, Z.; Ranjan, C.; van Gastel, M.; Schlögl, R. The Active Site for the Water Oxidising Anodic Iridium Oxide Probed through in Situ Raman Spectroscopy. *Chem. Commun. Camb* **2017**, *53* (92), 12414−12417.
(27) Pavlovic, Z.; Ranjan, C.; Gao, Q.; van Gastel, M.; Schlögl, R. Probing the Structure of a Water-Oxidizing Anodic Iridium Oxide Catalyst Using Raman Spectroscopy. *ACS Catal.* **2016**, *6* (12), 8098−8105.
(28) Kuo, D. Y.; Kawasaki, J. K.; Nelson, J. N.; Kloppenburg, J.; Hautier, G.; Shen, K. M.; Schlom, D. G.; Suntivich, J. Influence of Surface Adsorption on the Oxygen Evolution Reaction on IrO2(110). *J. Am. Chem. Soc.* **2017**, *139* (9), 3473−3479.
(29) Pfeifer, V.; Jones, T. E.; Velasco Velez, J. J.; Massue, C.; Greiner, M. T.; Arrigo, R.; Teschner, D.; Girgsdies, F.; Scherzer, M.; Allan, J.; Hashagen, M.; Weinberg, G.; Piccinin, S.; Havecker, M.; Knop-Gericke, A.; Schlögl, R. The Electronic Structure of Iridium Oxide Electrodes Active in Water Splitting. *Phys. Chem. Chem. Phys.* **2016**, *18* (4), 2292−2296.
(30) Pedersen, A. F.; Escudero-Escribano, M.; Sebok, B.; Bodin, A.; Paoli, E.; Frydendal, R.; Friebel, D.; Stephens, I. E. L.; Rossmeisl, J.; Chorkendorff, I.; Nilsson, A. Operando XAS Study of the Surface Oxidation State on a Monolayer IrOx on RuOx and Ru Oxide Based Nanoparticles for Oxygen Evolution in Acidic Media. *J. Phys. Chem. B* **2018**, *122* (2), 878−887.
(31) Sanchez Casalongue, H. G.; Ng, M. L.; Kaya, S.; Friebel, D.; Ogasawara, H.; Nilsson, A. In Situ Observation of Surface Species on Iridium Oxide Nanoparticles during the Oxygen Evolution Reaction. *Angew. Chem., Int. Ed. Engl.* **2014**, *53* (28), 7169−7172.
(32) Gottesfeld, S.; McIntyre, J. D. E.; Beni, G.; Shay, J. L. Electrochromism in Anodic Iridium Oxide Films. *Appl. Phys. Lett.* **1978**, *33* (2), 208−210.
(33) Pfeifer, V.; Jones, T. E.; Velasco Velez, J. J.; Arrigo, R.; Piccinin, S.; Havecker, M.; Knop-Gericke, A.; Schlögl, R. In Situ Observation of Reactive Oxygen Species Forming on Oxygen-Evolving Iridium Surfaces. *Chem. Sci.* **2017**, *8* (3), 2143−2149.
(34) Pfeifer, V.; Jones, T. E.; Wrabetz, S.; Massue, C.; Velasco Velez, J. J.; Arrigo, R.; Scherzer, M.; Piccinin, S.; Havecker, M.; Knop-Gericke, A.; Schlögl, R. Reactive Oxygen Species in Iridium-Based OER Catalysts. *Chem. Sci.* **2016**, *7* (11), 6791−6795.
(35) Monk, P. M. S.; Mortimer, R. J.; Rosseinsky, D. R. Electrochromism: Fundamental and Applications. *VCH* **1995**, 57−64.
(36) Minguzzi, A.; Locatelli, C.; Lugaresi, O.; Achilli, E.; Cappelletti, G.; Scavini, M.; Coduri, M.; Masala, P.; Sacchi, B.; Vertova, A.; Ghigna, P.; Rondinini, S. Easy Accommodation of Different Oxidation States in Iridium Oxide Nanoparticles with Different Hydration Degree as Water Oxidation Electrocatalysts. *ACS Catal.* **2015**, *5* (9), 5104−5115.
(37) Saveleva, V. A.; Wang, L.; Teschner, D.; Jones, T.; Gago, A. S.; Friedrich, K. A.; Zafeiratos, S.; Schlögl, R.; Savinova, E. R. Operando Evidence for a Universal Oxygen Evolution Mechanism on Thermal and Electrochemical Iridium Oxides. *J. Phys. Chem. Lett.* **2018**, *9* (11), 3154−3160.
(38) Kötz, R.; Neff, H.; Stucki, S. Anodic Iridium Oxide Films. XPS-Studies of Oxidation State Changes and O2-Evolution. *J. Electrochem. Soc.* **1984**, *131*, 72−77.
(39) Kötz, E. R.; Neff, H.; Müller, K. A UPS, XPS and Work Function Study of Emersed Silver, Platinum and Gold Electrodes. *J. Electroanal. Chem. Interfacial Electrochem.* **1986**, *215* (1−2), 331−344.
(40) Monk, P. M. S.; Mortimer, R. J.; Rosseinsky, D. R. Electrochromism and Electrochromic Devices. *Camb. Univ. Press* **2008**, 196−198.
(41) Robin, M. B.; Day, P. Mixed Valence Chemistry-A Survey and Classification. *Adv. Inorg. Chem. Radiochem.* **1968**, *10*, 247−422.
(42) Gottesfeld, S.; McIntyre, J. D. E. Electrochromism in Anodic Iridium Oxide Films. II. PH Effects on Corrosion Stability and the Mechanism of Coloration and Bleaching. *J. Electrochem. Soc.* **1979**, *126*, 742−750.
(43) Ledendecker, M.; Geiger, S.; Hengge, K.; Lim, J.; Cherevko, S.; Mingers, A. M.; Göhl, D.; Fortunato, G. V.; Jalalpoor, D.; Schüth, F.; Scheu, C.; Mayrhofer, K. J. J. Towards Maximized Utilization of Iridium for the Acidic Oxygen Evolution Reaction. *Nano Res.* **2019**, *12* (9), 2275−2280.
(44) Kasian, O.; Grote, J. P.; Geiger, S.; Cherevko, S.; Mayrhofer, K. J. J. The Common Intermediates of Oxygen Evolution and Dissolution Reactions during Water Electrolysis on Iridium. *Angew. Chem., Int. Ed. Engl.* **2018**, *57* (9), 2488−2491.
(45) Cherevko, S.; Geiger, S.; Kasian, O.; Mingers, A.; Mayrhofer, K. J. J. Oxygen Evolution Activity and Stability of Iridium in Acidic Media. Part 2. − Electrochemically Grown Hydrous Iridium Oxide. *J. Electroanal. Chem.* **2016**, *774*, 102−110.
(46) Sharninghausen, L. S.; Bhushan Sinha, S.; Shopov, D. Y.; Mercado, B. Q.; Balcells, D.; Brudvig, G. W.; Crabtree, R. H. Synthesis and Characterization of Iridium (V) Coordination Complexes With an N, O-Donor Organic Ligand. *Angew. Chem.* **2017**, *129*, 13227−13231.
(47) Sinha, S. B.; Shopov, D. Y.; Sharninghausen, L. S.; Stein, C. J.; Mercado, B. Q.; Balcells, D.; Pedersen, T. B.; Reiher, M.; Brudvig, G. W.; Crabtree, R. H. Redox Activity of Oxo-Bridged Iridium Dimers in an N,O-Donor Environment: Characterization of Remarkably Stable Ir(IV,V) Complexes. *J. Am. Chem. Soc.* **2017**, *139* (28), 9672−9683.
(48) Lang, C.; Li, J.; Yang, K. R.; Wang, Y.; He, D.; Thorne, J. E.; Croslow, S.; Dong, Q.; Zhao, Y.; Prostko, G.; Brudvig, G. W.; Batista, V. S.; Waegele, M. M.; Wang, D. Observation of a Potential-Dependent Switch of Water-Oxidation Mechanism on Co-Oxide-Based Catalysts. *Chem.* **2021**, *7*, 2101.
(49) Balzani, V.; Campagna, S.; Barbieri, A.; Barigelletti, F.; Cheng, E. C.-C.; Flamigni, L.; Gunnlaugsson, T.; Kirgan, R. A.; Kumaresan, D.; Leonard, J. P.; Nolan, C. B.; Rillema, D. P.; Sabatini, C.; Schmehl, R. H.; Shankar, K.; Stomeo, F.; Sullivan, B. P.; Vaidya, S.; Ventura, B.; Williams, J. A. G.; Yam, V. W.-W. Photochemistry and Photophysics of Coordination Compounds II. *Springer Top. Curr. Chem.* **2007**, *281*, 143−203.
(50) Balzani, V.; Campagna, S.; de Meijere, A.; Houk, K. N.; Kessler, H.; Lehn, J.-M.; Ley, S. V.; Schreiber, S. L.; Thiem, J.; Trost, B. M.; Vögtle, F.; Yamamoto, H. Photochemistry and Photophysics of Coordination Compounds I. *Springer Top. Curr. Chem.* **2007**, *280*, 1−36.
(51) Rossmeisl, J.; Qu, Z. W.; Zhu, H.; Kroes, G. J.; Nørskov, J. K. Electrolysis of Water on Oxide Surfaces. *J. Electroanal. Chem.* **2007**, *607* (1−2), 83−89.
(52) Liu, J. Catalysis by Supported Single Metal Atoms. *ACS Catal.* **2017**, *7* (1), 34−59.
(53) Lin, J.; Wang, A.; Qiao, B.; Liu, X.; Yang, X.; Wang, X.; Liang, J.; Li, J.; Liu, J.; Zhang, T. Remarkable Performance of Ir1/FeOx Single-Atom Catalyst in Water Gas Shift Reaction. *J. Am. Chem. Soc.* **2013**, *135* (41), 15314−15317.
(54) Giannakakis, G.; Flytzani-Stephanopoulos, M.; Sykes, E. C. H. Single-Atom Alloys as a Reductionist Approach to the Rational Design of Heterogeneous Catalysts. *Acc. Chem. Res.* **2019**, *52* (1), 237−247.
(55) Yang, X.-F.; Wang, A.; Qiao, B.; Li, J.; Liu, J.; Zhang, T. Single-Atom Catalysts: A New Frontier in Heterogeneous Catalysis. *Acc. Chem. Res.* **2013**, *46*, 1740−1748.

https://doi.org/10.1021/jacs.2c02006
J. Am. Chem. Soc. 2022, 144, 8454−8459